Journal of Nuclear Materials 390–391 (2009) 465–469

Contents lists available at ScienceDirect

Journal of Nuclear Materials

journal homepage: www.elsevier.com/locate/jnucmat

Main chamber high recycling on ASDEX upgrade

K. McCormick *, R. Dux, R. Fischer, A. Scarabosio, The ASDEX Upgrade Team

Max-Planck-Institut für Plasmaphysik, EURATOM, 85748 Garching, Germany

ARTICLE INFO

PACS:
52.25.Ya
52.40.Hf
52.25.−b
52.55.Fa

ABSTRACT

Main chamber recycling has been quantified over a wide range (I_p = 0.6–1.1 MA, B_t = −3 to −1.9 T, n_e = 0.3–1 × 10^{20} m^{-3}, P_{tot} = 2.5–20 MW), both inter-ELM and during type-I ELMs. A vertical CO_2 interferometer channel registers densities δn_eLV2 in excess of those expected from core/SOL parameters. δn_eLV2 is localized at the inner, lower divertor baffle in the main chamber. Its behavior follows the neutral fluxes measured by a nearby pressure gauge. Particle fluxes to the inner wall as well as densities exhibit parallel behavior. δn_eLV2 can be as high as 8 × 10^{19} m^{-2} and the ELM perturbation itself as large as 9 × 10^{19} m^{-2}. n_e at the inner wall reaches 2.5 × 10^{20} m^{-3} and fluxes ∼6 × 10^{23} s^{-1}. For controlled conditions δn_eLV2 is linear with n_e and increases with P_{tot}. A n_e threshold increasing with I_p exists below which δn_eLV2 ∼ 0, corresponding to a Greenwald density <0.45. These results suggest enhanced SOL transport, both inter-ELM and during ELMs, on the high field side leading to these appreciable plasma-wall interactions.

1. Introduction

On ASDEX Upgrade (AUG) main chamber recycling (MCR) is commonly registered on the high field side (HFS) at the inner heat shield (HS) and lower divertor baffle in the light of D_α observed by video cameras. Whereas such observations are of qualitative nature, they are nonetheless surprising since the separatrix-wall distance can be large. In any case, the potential importance to ITER of high fluxes to plasma-facing components in the main chamber [1] warrants more detailed investigation of the observations on AUG in addition to work already published [2]. This paper reports on observations made by the innermost vertical interferometer channel and a main chamber pressure gauge behind the HS. These are brought into connection with particle flux measurements over the HS as well as new density determinations there via the Stark effect.

MCR has been extensively investigated on Alcator C-Mod [3] where it is found that it can be dominant over fluxes to the divertor and is attributed to enhanced transport in the far SOL, thereby leading to a stronger plasma-wall interaction than otherwise expected. Studies on AUG found MCR of importance and HFS fluxes larger [2]. As on C-MOD [4], the main chamber neutral pressure was found to be largely determined by MCR rather than by leaks through divertor bypasses or the divertor plasma.

On DIII-D a CO_2 interferometer chord passing through the core plasma and intersecting the outer SOL plasma (r_{sol} < 1 cm) at the target plate showed a large density perturbation (2 × 10^{20} m^{-3}) associated with an ELM, explained by local recycling processes in the divertor [5]. The difference between the DIII-D results and those of AUG is that much greater density excursions are seen and they are: (a) in the far SOL, (b) on the HFS and (c) in the main chamber. Further, these densities are observed steady-state as well, with an ELM contribution on top. On JT-60 ELM-associated density perturbations were registered by a CO_2 interferometer passing through the inner periphery of the core plasma and intersecting the inner divertor baffle, a situation similar to that on AUG [6]. δn_eLELM ⩽ 2 × 10^{19} m^{-2} was found, not unlike AUG.

2. Experiment

The results presented are for D^+ H-mode plasmas and were obtained with W-covered walls and mostly carbon divertor target plates with varying degrees of wall conditioning and boronization. However, recent discharges in the all-W machine with no boronization show the same tendencies. None of the discharges in the assembled database are dedicated to the task of this paper, meaning that often several potentially important parameters are changing at the same time. Thus the high-power NBI scans up to 20 MW are carried out in steps of only a few 100 ms length and from step to step the lower triangularity δ_l, n_e and distances to the wall can vary. Nonetheless these results fall into the same pattern seen for steady-state under more controlled conditions. Discharges with varying degrees of detachment at the inner and outer divertor do not appear to affect correlations among main chamber signals. Generally the last limiting SOL flux surface (FSlim) rests on the inner heat shield, but not always uniformly, and in a few cases is determined by structures on the low field side (LFS). The Bx∇B

* Corresponding author.
E-mail address: gkm@ipp.mpg.de (K. McCormick).

0022-3115/$ - see front matter © 2009 Published by Elsevier B.V.
doi:10.1016/j.jnucmat.2009.01.145

drift is directed towards the lower x-pt. Thus SOL plasma drifts can potentially lead to a 'broadening' of the SOL on the HFS.

2.1. Diagnostics

The principal investigative tool is the innermost vertical CO_2 interferometer channel (V2), measuring the line integral density n_eLV2 along a chord intersecting a small portion of the core plasma (Fig. 1). Of interest is the difference between the value to be expected from core/SOL density profiles n_eLV2mod [7] and n_eLV2. This 'excess' density δn_eLV2 = n_eLV2 − n_eLV2mod is a measure of main chamber recycling. During an ELM the difference δn_eLV2ELM between the ELM peak and background is taken to characterize this density perturbation. ASDEX-type pressure gauges behind the HS (F11) and beneath the dome (F1, F4) and inner divertor (F19) permit a measure of recycling in those regions [8]. Particle fluxes deduced from D_γ measurements spanning the HS are available as well as local densities n_eHS at the HS determined by Stark broadening.

2.2. Inter-ELM (steady-state) results

Fig. 2 shows a comparison among the signals n_eLV2, n_eLV1 and the computed n_eLV2mod. It is apparent for $t > 2$s that n_eLV2 > n_eLV1, implying V2 is registering a steady-state density considerably greater than the core density of the plasma since the chord length for V1 is much greater than that of V2. δn_eLV2 increases from zero beginning ~1.7 s, peaks around 2.25 s and then falls back to a lower, constant level. The decrease in n_eLV2mod is related to a shift in plasma position (see R_{in} of Fig. 2) and concurrent reduction of the V2 chord length. The dome neutral flux F04 shows no correlation with this behavior, reacting principally to the increased P_{nbi} and then gas puff at ~2.32 s. In contrast a close correlation of δn_eLV2 with F11 is evident. The deviating behavior between F11 and F19 can be traced to configuration changes: At ~2.3 s the limiting SOL flux surface touches the lower edge of the HS (see Fig. 1), then relaxes to a situation where it is almost uniformly tangent. This implies that local recycling can be a dominanting effect for F11 rather than the bypass from F19 to F11.

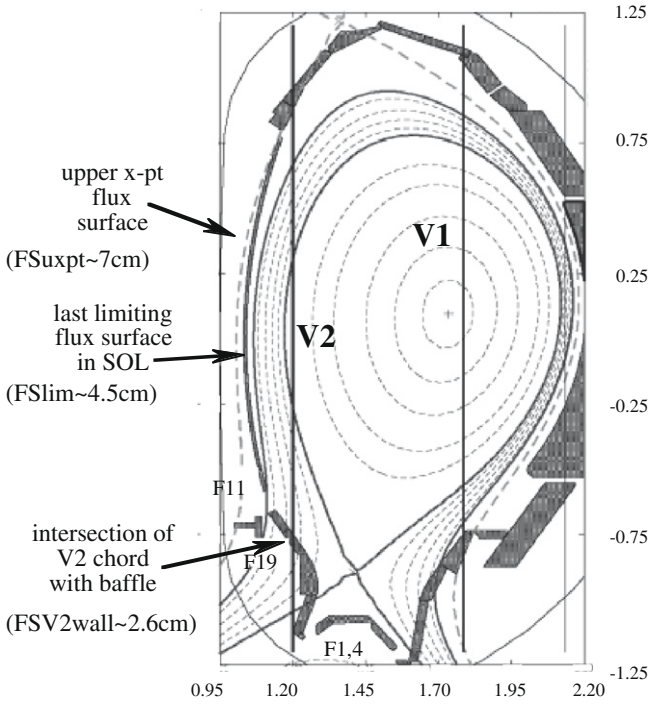

Fig. 1. Cross section of ASDEX-Upgrade showing the flux surfaces for #23009 at 2.3s, considered in Fig. 2. The position of the vertical CO_2 interferometer chords are indicated (V1 & V2) as well as the pressure gauges F1, 4 (dome), F19 (inner divertor) & F11 (HS). The SOL flux coordinates referenced to the outer midplane for the upper x-pt, limiting SOL flux surface and V2 at the wall are indicated.

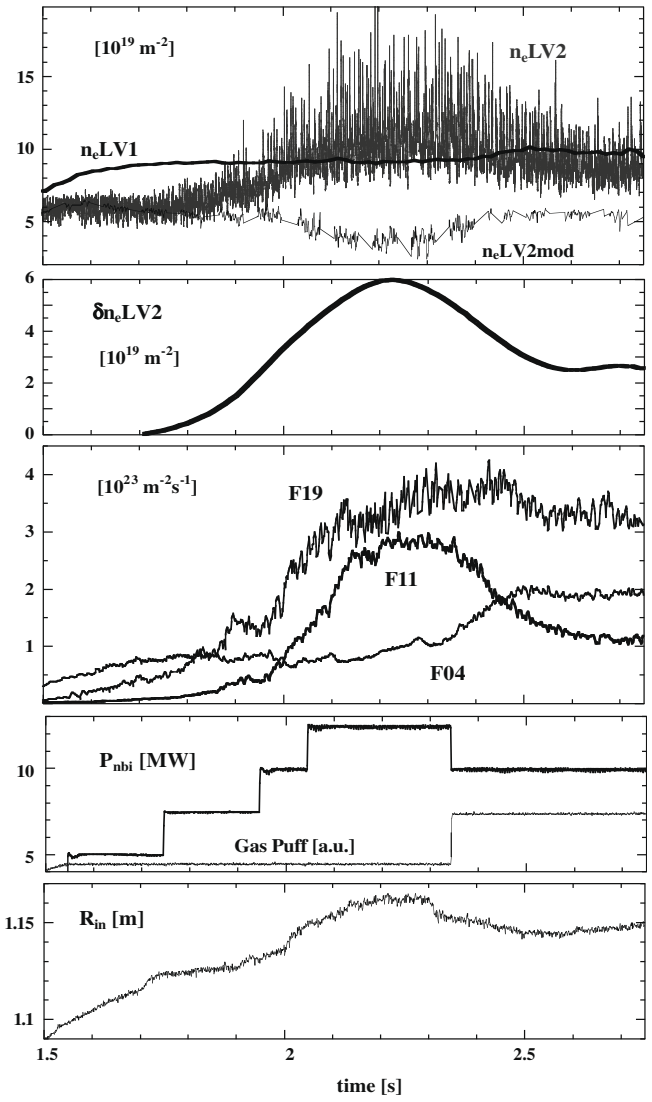

Fig. 2. Temporal behavior of (top to bottom): line-integrated density n_eL for interferometer channels V1 & V2 and predicted n_eLV2; δn_eLV2; neutral fluxes for gauges F04, F19 & F11; NBI power and gas injection waveform; and radial position R_{in} of innermost extent of the separatrix. Due to the R_{in} variation, the chord length of V2 within the core varies ~ 1–0.56 m over 1.5–2.3s. The distance between separatrix and lower edge of LHS is ~15–16.5 cm.

Fig. 3 considers six discharges (0.8 and 1 MA) where high MCR prevailed and n_eHS values at the heat shield were available. All quantities are plotted vs. F11 as this turns out to be a good ordering parameter for steady-state behavior. δn_eLV2 is well correlated with F11 over the range, but increases less than linearly. In contrast δn_eLV2ELM exhibits no relationship to F11 at all. The inner divertor neutral flux F19 is linear with F11 over a short range, indicating either that F19 is closely coupled to F11 through bypasses for these conditions or that recycling has a parallel behavior in the divertor and main chamber. However, at higher F11 there is no correspondence, showing that local recycling is making a larger contribution to F11 than F19. The particle fluxes to the HS are linear with F11 at low values and then show some scatter, again related to configuration effects not fully mirrored in F11. The combined HS flux (lower + upper) is in excess of 6×10^{23} s^{-1} (over ~8 m^2 surface) at the

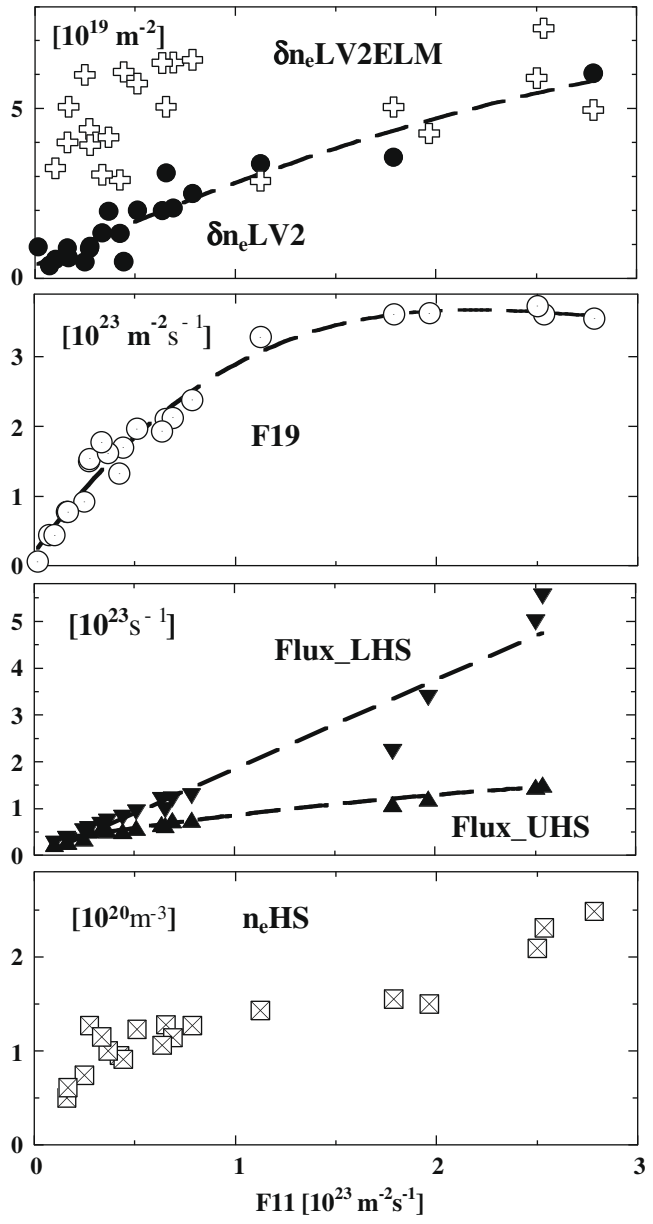

Fig. 3. Top to bottom, all vs. F11: δn_eLV2 & δn_eLV2ELM; F19; integral particle flux to upper & lower heat shields; density at end of lower heat shield from Stark broadening. Traces are to guide the eye only. #23009, 23069, 23081–82, 23084, 23086.

highest value, a remarkable recycling level considering that the HS is 15 cm distant from the separatrix at this point. Finally, the density n_eHS at the lower part of the heat shield also closely follows F11, ultimately reaching $\sim 2.5 \times 10^{20}$ m^{-3}.

The CO_2 interferometer registers line-integrated densities, without details as to the location of n_e and its spatial extent. H_α videos suggest this high n_e region is next to the divertor baffle. Thus if δn_eLV2 were concentrated in a region of 5 cm near the baffle, a local density of 1.2×10^{21} m^{-3} for the highest point in Fig. 3 would be indicated. On the other hand, if the density were evenly distributed between the separatrix and baffle, $n_e \sim 1.2 \times 10^{20}$ m^{-3} would result, less than n_eHS. However, the distance between the separatrix and intersection of V2 with the baffle varies over 0.25–0.5 m in the time 1.7–2.3 of Fig. 2, which would lead to a 'local density' varying in an entirely different fashion than any of the other signals. It would also lead to n_e in the near SOL in excess of the core density. These considerations suggest the registered n_e lies near the baffle.

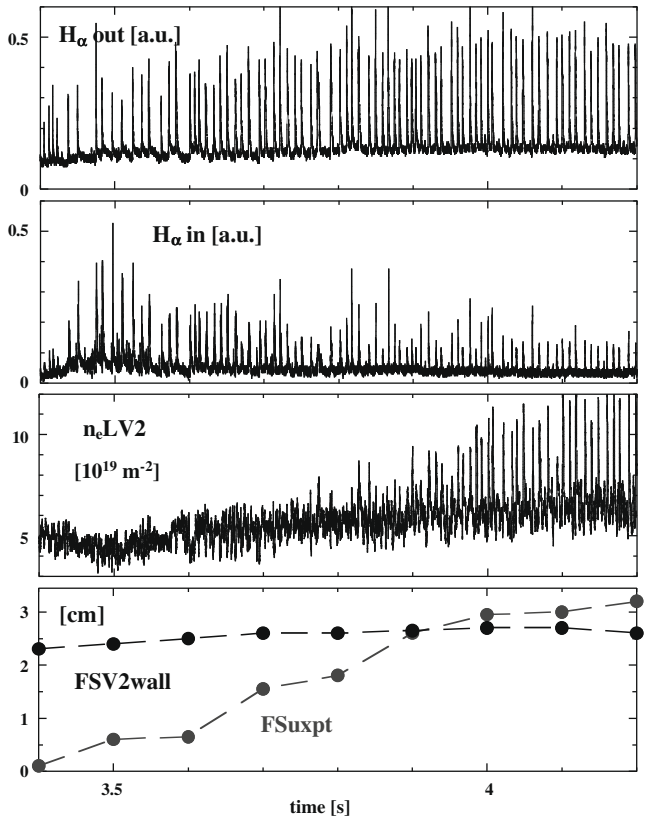

Fig. 4. Temporal behavior of H_α at the outer and inner divertor & n_eLV2 during a transition from a DN to a LSN configuration. Bottom: FSV2wall (nearly constant) & FSuxpt (increasing values => upper x-pt shadow is progressing into SOL). V2 ELM activity becomes evident ~3.8s and fully developed ~3.9s where FSV2wall no longer lies within the shadow of the upper x-pt. #18578, $n_e \sim 6.3$–7.7×10^{19} m^{-3}, P_{nbi} = 5 MW.

Fig. 4 explores this point by documenting the H_α behavior at the inner and outer divertors as well as n_eLV2 during a transition from a double null ($t \sim 3.4$ s) to a LSN configuration. The bottom plot gives the position of SOL flux surface coordinate of the upper x-point FSuxpt during this transition. ELM activity at the outer divertor is established $t < 3.4$ s in the position scan, indicating that shadowing of the outer divertor by the upper x-pt is almost immediately ineffective. H_{α_in} begins to register ELMs when FSuxpt~0.5 cm, i.e. the particle and energy fluxes associated with an ELM originating at the outer midplane are already in complete contact with the inner divertor for $t \geqslant 3.5$ s. In contrast, the ELMs seen by n_eLV2 do not make their appearance until ~3.8–3.9 s, at which point FSuxpt begins to cross the intersection of V2 with the baffle. Since prior to this point the flux surfaces inside FSuxpt are in unhindered communication with the SOL on the LFS and V2 nonetheless does see any ELM activity, we conclude that at least the ELM signatures registered by V2 must be near the baffle.

Fig. 5 summarizes the systematic change of δn_eLV2 vs. F11, n_e and n_eGW for the entire database, with I_p as a parameter. (The 0.6MA discharges have P_{nbi} = 5 MW and represent the closest situation to a controlled n_e-scan.) The parallel behavior of F11 and δn_eLV2 is striking considering the variety of conditions. What appears to be scatter in the data is actually systematic, i.e. the lower values for δn_eLV2 originate from a few discharges whose behavior is quite coherent with F11, they simply lie below the other points. Plotting this data as a function of n_e reveals an apparent I_p-dependent density threshold, above which the potential to attain high δn_eLV2 increases. Within the 0.6 MA dataset the variation occurs due to a change in n_e. For 0.8 & 1 MA there are no n_e scans where

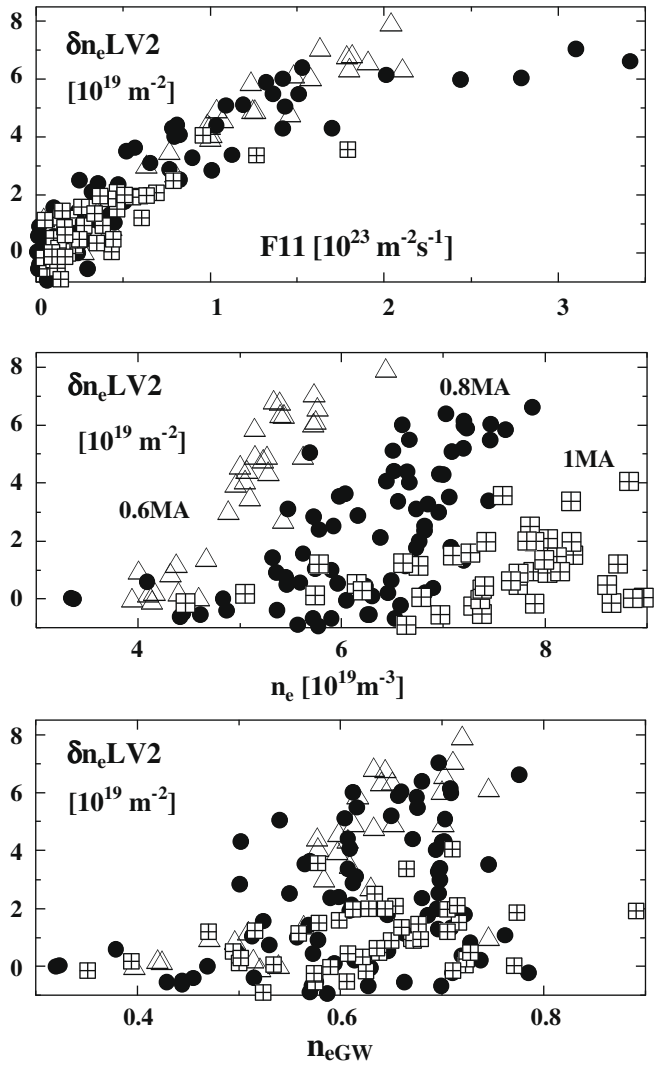

Fig. 5. Top: δn_eLV2 vs. F11, demonstrating the close relationship for all conditions (I_p = 0.6MA triangles, 0.8 MA circles, 1.1MA squares, B_t = −1.9 to −3T, $\delta_l \sim$ 0.3–0.5, P_{tot}~2.5–20 MW). Middle: Same data vs. line-averaged density, showing how the n_e threshold increases with I_p. Bottom: Same data vs. n_{eGW}.

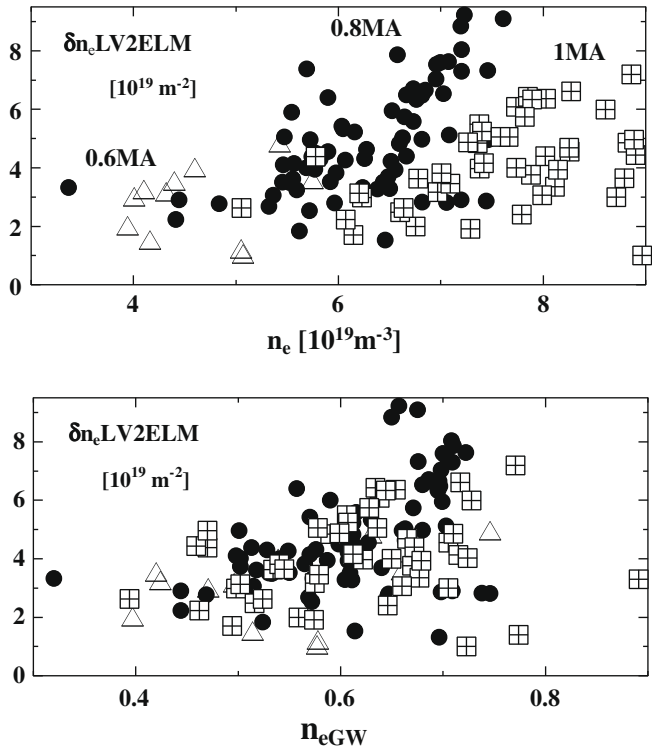

Fig. 6. δn_eLV2ELM vs. line-averaged density (top) and n_{eGW} (bottom). As for δn_eLV2 of Fig. 5, the highest values are found at high n_e and P_{tot}.

everything else is kept constant. But power scans do exist, showing that δn_eLV2 increases with P_{tot}. Indeed at $P_{tot} \sim 2.5$ MW for 0.8 MA δn_eLV2 is in the 'noise level' of $\sim\pm 10^{19}$ m^{-2}, as are most of the 5 MW discharges (but not all). All 0.8MA points with δn_eLV2 > 3×10^{19} m^{-2} are associated with $P_{tot} \geqslant 10$ MW. There is no clear dependence for δn_eLV2 on FSV2wall or distances to the wall or position of inner separatrix (FSV2wall ~ 2–5 cm, FSlim ~ 2–6 cm, R_{in}~1.1–1.22 m, respectively) which may be due to colinearities arising from non-controlled variations of leading parameters. Plotting the same data as a function of the Greenwald density n_{eGW}, leads to a rather surprising complete overlay of the operational points and shows that the Greenwald-normalized 'threshold density' is ~0.45.

2.3. ELM Behavior

From Fig. 3 we know that δn_eLV2ELM can attain very high values and from the USN → LSN scan of Fig. 4 that these density perturbations are located near the baffle. Details as to the extent of ELM penetration into the SOL or waveform vs. operational parameters is too complex to consider here. Suffice it to say that the temporal behavior of the ELM perturbation can be very similar to that of outer H_α in terms of rise time (<0.1 ms) and decay (<1 ms) but this behavior is not universal. Fig. 3 has also demonstrated that steady-state recycling of which F11 is indicative is not related to the ELM amplitude, implying that ELMs make no substantial contribution to the background neutral pressure. Otherwise δn_eLV2ELM appears to underlie similar dependencies as δn_eLV2, i.e. increase with n_e and power, but again the lack of coherent scans makes it impossible to collate the behavior in the sense of a scaling. Fig. 6 displays δn_eLV2ELM for the dataset of Fig. 5 vs. n_e and n_{eGW}. Once again an I_p-dependent density threshold emerges for larger δn_eLV2ELM, and these points also coalesce when plotted vs. n_{eGW}. δn_eLV2ELM varies over 1–9 $\times 10^{19}$ m^{-2}. Even assuming the high density region seen by V2 is as large as 10 cm rather than being localized near the baffle, implies that δn_eV2ELM ~9×10^{20} m^{-2}.

3. Discussion

It has been demonstrated that the steady-state excess density measured along the V2 chord δn_eLV2 is well correlated with signals from a nearby pressure gauge situated behind the HS and that these signals show a strong relationship to particle fluxes at the HS as well as densities measured there. Further it is established that these signals are not governed by the pressure under the dome (gauges F1 or F4) and are not always tied to the pressure in the inner divertor, all of which points to particle and power fluxes penetrating into the far SOL of magnitude such as to effect the observed phenomena. This level of MCR is consistent with observations on AUG in the past and with those of C-MOD except now absolute numbers are associated with the observations and are clearly located on the HFS.

A particularly intensive plasma-wall interaction on the HFS is not expected since this is a region of good curvature. Drifts driven by poloidal T_e-gradients along field lines could be a candidate, in particular since they would also exhibit an I_p-dependence consistent with that seen. However, since these gradients will not be

large in the far SOL such a mechanism is necessarily confined to the near SOL, meaning that enhanced transport in the far SOL must be postulated in addition. To this end, exploratory modeling with SOLPS5 for OH discharge conditions with enhanced SOL diffusive transport shows little difference between inclusion of drift effects or not [9]. SOLPS5 calculations with drifts under the H-mode conditions discussed here remain yet to be done.

It is notable that the phenomenological behavior of δn_eLV2 and δn_eLV2ELM underlies similar boundaries, i.e. an n_e threshold increasing with I_p which can be collapsed into one operational regime when considered in terms of n_{eGW}. This might be indicative that basic processes governing both steady-state and ELM transport have similarities, at least in the far SOL. Since ELM transport is not of diffusive nature, we might conclude that steady-state transport is also convective in nature, with this transport becoming increasingly virulent with increasing n_{eGW}.

4. Conclusion

Main chamber recycling, inter-ELM and at ELMs, has been studied over a wide range of H-mode conditions (I_p = 0.6–1.1 MA, $B_t = -3$ to –1.9T, n_e = 0.3–1 $\times 10^{20}$ m^{-3}, P_{tot} = 2.5–20 MW, $\delta_l \sim$ 0.3–0.45) using an in-vessel pressure gauge and CO_2 interferometer (measuring n_eL) as the principal instruments for documentation on the high field side. Neutral fluxes up to 3.5 $\times 10^{23}$ m^{-2} s^{-1} are found, along with n_eL $\sim 8 \times 10^{19}$ m^{-2} located in the vicinity of the baffle. Total particle fluxes up to 6×10^{23} s^{-1} have been registered over the inner heat shield (from $D\gamma$), where n_e can attain 2.5 $\times 10^{20}$ m^{-3} (from Stark effect). All these quantities are well correlated, indicating for the most part that high main chamber neutral pressures are indeed indicative of high MCR and there can be no question of leaks from the divertor being singularly responsible for the pressures. The numbers quoted are remarkable as the heat shield can be at considerable distance from the separatrix, implying substantial cross-field transport in the far SOL. New is the systematic inter-ELM (steady-state) quantification of the associated plasma-wall interaction and the considerable magnitudes of such on the HFS. The values at an ELM are equally substantial, albeit perhaps less surprising since this is a recognized issue and under intensive study.

The fluxes and densities increase with heating power and density, exhibiting an I_p-dependent density threshold above which they can become increasingly significant. Plotting the neutral fluxes and excess densities vs. n_{eGW} causes the operational regions for different currents to coalesce, both for steady-state and ELM observations. This intriguing result may imply a Greenwald-related enhanced transport onset condition (here $n_{eGW} \sim 0.45$) heretofore undocumented and could have implications for ITER which is foreseen to operate near $n_{eGW} \sim 1$. More detailed investigations under controlled conditions are necessary.

References

[1] B. Lipschultz et al., NF47 (2007) 1189.
[2] A. Kallenbach et al., NF 43 (2003) 573.
[3] B. LaBombard et al., NF 40 (2000) 2041.
[4] B. Lipschultz et al., PPCF 44 (2002) 733.
[5] A.W. Leonard et al., J. Nucl. Mater. 313–316 (2003) 768.
[6] A.V. Chankin et al., J. Nucl. Mater. 313–316 (2003) 828.
[7] R. Fischer et al., Plasma Physics and Controlled Fusion, in press.
[8] A. Scarabosio et al., J. Nucl. Mater. 390–391 (2009) 494.
[9] M. Wischmeier et al., J. Nucl. Mater. 390–391 (2009) 250.